RBR

Dynamic corrections for the RBRargo CTD 2000dbar

1 Summary

Dynamic corrections refer to adjustments that must be made to measured conductivity and temperature to account for a variety of errors that are caused by sampling in a dynamic environment. In the context of a profiling instrument, environmental variability is caused by the instrument's motion through spatial temperature and salinity gradients. The source of the dynamic errors and corrective actions are not unique to the RBR*argo* inductive CTD; the same physics applies to electrode-based CTDs.

Dynamic errors in conductivity and temperature are usually small relative to natural variations. However, they sometimes compound into large *relative* errors in derived variables such as salinity and density because, in many regions of the ocean, salinity and density do not vary as much as conductivity and temperature. Dynamic errors often create signatures of density instability in profiles, falsely implying that there was active mixing.

The RBR*argo* inductive conductivity cell is calibrated to an initial accuracy of ±0.003mS/cm, and has a resolution of 0.001mS/cm. In some circumstances, the dynamic errors can significantly exceed the calibration accuracy, and therefore it is very important to correct for them.

This report begins with a discussion of the source of dynamic errors in both conductivity and temperature, and how the errors manifest when deriving salinity. Then we present a method to correct for each of the dynamic errors for the specific case of a float ascending at 10cm/s with an RBR*argo* "combined" CT cell. We then quantify the free parameters in the corrections with in situ float data and laboratory experiments. A short discussion follows on the merits of correcting dynamic errors on-board in contrast to correcting errors in post-processing, and finally, we provide a Matlab code example to illustrate how the corrections can be applied to float data in post-processing.

The corrections we propose are the following:

1. Advance temperature in time by 0.3s.
2. Apply the long-term thermal correction to conductivity ($\tau = 60$s).
3. Apply the Morison et al. (1994) version of the Lueck and Picklo (1990) correction for conductivity cell thermal inertia: $\alpha = 0.08$, $\beta = 0.125 s^{-1}$ ($\tau = 8$s).

2 Introduction to dynamic corrections

2.1 Short-term dynamic errors

A short-term dynamic error is defined here as an error occurring over a characteristic time scale of a second or less. A number of factors govern the short-term dynamic response of conductivity cells and thermistors:

1. Spatial separation on the CTD
2. Spatial averaging
3. Sensor response time

There is a rich literature detailing different methods to correct for each of these problems on various CTDs, however, they do not deal with the specific case of an RBR inductive conductivity cell. Below we briefly discuss each factor in general terms, but then consider how they are relevant in the context of an RBR*argo* CTD sampling at 1Hz or less on an autonomous float ascending at 10cm/s.

2.1.1 Conductivity and temperature spatial separation

When a conductivity cell and thermistor are not colocated on a profiling instrument, they effectively measure the same water parcel but at different times. In a freely flushing instrument, the time difference between the measurements depends on flow speed and distance between the sensors. A variable profiling rate therefore causes a variable time difference, which in principle makes a time lag correction difficult. Enclosing the sensors in a duct and pumping water past them at a known rate is one way to solve the problem. However, the variable lag issue was solved without pumps when RBR introduced the "combined CT cell" in 2016 (Fig. 1). In this design, the thermistor was moved from the float end cap to the mast of the conductivity cell, reducing errors caused by vertical sensor misalignment.

Fig. 1 The 2000dbar RBR combined conductivity-temperature (CT) cell. The temperature sting is vertically aligned with the conductivity cell, minimizing errors caused by CT separation.

2.1.2 Spatial averaging

The sensing volume of the RBR inductive conductivity cell is different from the thermistor. The conductivity cell itself is 4.7cm in length, but it has an effective sensing radius of about 15cm due to the basic nature of inductive conductivity cells. Although the cell's effective sampling radius is 15cm, the measurement is weighted most heavily by the sample

water inside the cell where the induced current density is highest. Careful in situ measurements have shown that sharp gradients as thin as 10cm can be resolved with the same precision as a pumped system.

In contrast, the sensing element of the thermistor assembly is a very small semiconductor embedded into a 2.5mm wide titanium housing or "sting." In relative terms, temperature is a point measurement compared to conductivity.

The finite extent of the induced current field and the position of the thermistor means that the conductivity cell will register a change both before and after the thermistor does. In other words, there is vertical symmetry in the arrangement. By this reasoning, there should be no delay between conductivity and temperature, and neither sensor requires a time shift to compensate for spatial response.

2.1.3 Sensor response time

Thermistors and conductivity cells have finite, but different, response times. Heat must diffuse through a metal housing to reach the thermistor itself before a temperature change is registered. If a sensor has a long response time relative to the time scale for temperature changes, then the measured temperature will both lag the true signal, and have a reduced high-frequency amplitude. As the time constant increases, the lag and high-frequency attenuation increase. Mathematically, the measured temperature is a convolution of the sensor response with the true marine temperature. In most CTDs, including the RBR*argo* CTD, the conductivity cell reacts more quickly than the thermistor. The thermistors on RBR*argo* CTDs have a measured time constant of 700ms. We will show later that the lag caused by the finite time response is important even when sampling at 1Hz.

The response time of the conductivity cell is more difficult to characterize. It is an electrical measurement, and thus does not require diffusion of a substance or property through a medium in the same way that a thermistor or oxygen optode does. By that reasoning, the response time is likely faster than the thermistor. However, conductivity is a function of temperature (and salinity), and dynamic errors occur when the cell exchanges heat with the water it samples. The time scale for this adjustment is longer than one second, and is therefore discussed in the next section on medium and long-term dynamic errors.

2.2 Medium and long-term dynamic errors

While variations in temperature have consequences for temperature and pressure, the impacts are greatest on conductivity. In much of the ocean, salinity variations are relatively weak, which means that conductivity is determined primarily by temperature. Dynamic thermal errors impact measured conductivity, and these translate into errors when salinity and density are computed. The conductivity error can be 0.01mS/cm or more depending on the ambient temperature gradient and profiling rate.

As we will show, the RBR conductivity cell can be characterized by two thermal adjustment time scales: approximately ten seconds and sixty seconds. These adjustments are the cause of the what we refer to as the thermal medium-term and long-term dynamic conductivity errors.

Dynamic conductivity errors are caused by thermal contamination of the sample seawater in the vicinity of the conductivity cell. Heat exchange between the sample water and instrument changes the water conductivity, and hence any parameter derived from conductivity. The error can manifest itself in different ways. For example, there may be spikes in salinity and density when the instrument enters a mixed layer from stratified water, or there may be a consistent bias in regions that are continuously stratified.

Lueck (1990) analyzed the thermal inertia of the conductivity cell analytically, and Lueck and Picklo (1990) compared the analytical results with in situ data from the Caribbean Sea thermohaline staircase. Lueck and Picklo (1990) also developed a regressive conductivity correction term to estimate the true conductivity from measured conductivity. The discrete form of the equation to compute the conductivity error is:

$$C_T(n) = -bC_T(n-1) + \gamma a[T(n) - T(n-1)]$$
$$a = 4f_N\alpha\beta^{-1}(1 + 4f_N\beta^{-1})^{-1}$$
$$b = 1 - 2a\alpha^{-1}$$

In this equation, $C_T(n)$ is the conductivity error that must be *added* to the measured conductivity to arrive at a corrected value, i.e.,

$$C_{cor}(n) = C(n) + C_T(n)$$

where T is the measured temperature (marine temperature), γ is a scale factor that converts the temperature gradient to a conductivity gradient (1mS/cm/°C for most seawater), f_N is the Nyquist frequency ($f_S/2$), α is the initial volume-weighted thermal anomaly, and β is the inverse time constant for the adjustment. The temperature used in this equation should be the free-stream temperature of the fluid inside the cell. This measurement is not available, and so we, like others, use the temperature measured by the marine thermistor as a proxy for the free-stream temperature. Ideally the marine temperature should be "sharpened" and/or aligned to account for its own thermal lag and any other lag caused by spatial separation (e.g. Johnson et al., 2007).

2.3 Conductivity and temperature response matching

Matching the time response of the conductivity cell and thermistor is difficult because each responds differently to temperature gradients. The implication of mismatched measurements is apparent in derived parameters. The most common and easily recognizable error is salinity spiking at sharp temperature interfaces, although it is important to recognize that under continuous stratification the error will be in the form of a bias instead of spikes, and this error is much more difficult to detect.

2.4 Uncorrected data example: salinity and density

In August 2017, the US Naval Academy and the Woods Hole Oceanographic Institution air-deployed an MRV Systems ALAMO float (#9139) with an RBR*argo* CTD from a US Air Force Hurricane Hunter aircraft into the Caribbean Sea south of Puerto Rico. The float profiled on ascent at a nominal rate of 10cm/s repeatedly from a parking depth of about 500m to the surface. Many of the profiles profiled through a thermohaline staircase. The profiles contain as many as ten steps that have uniformly mixed layers 5 to 20m thick separated by stratified interfaces less than 1m thick.

Thermohaline staircases are ideal for studying dynamic errors in CTD data; in fact, Lueck and Picklo (1990) used data from this same region to develop corrective algorithms for dynamic errors in temperature and conductivity.

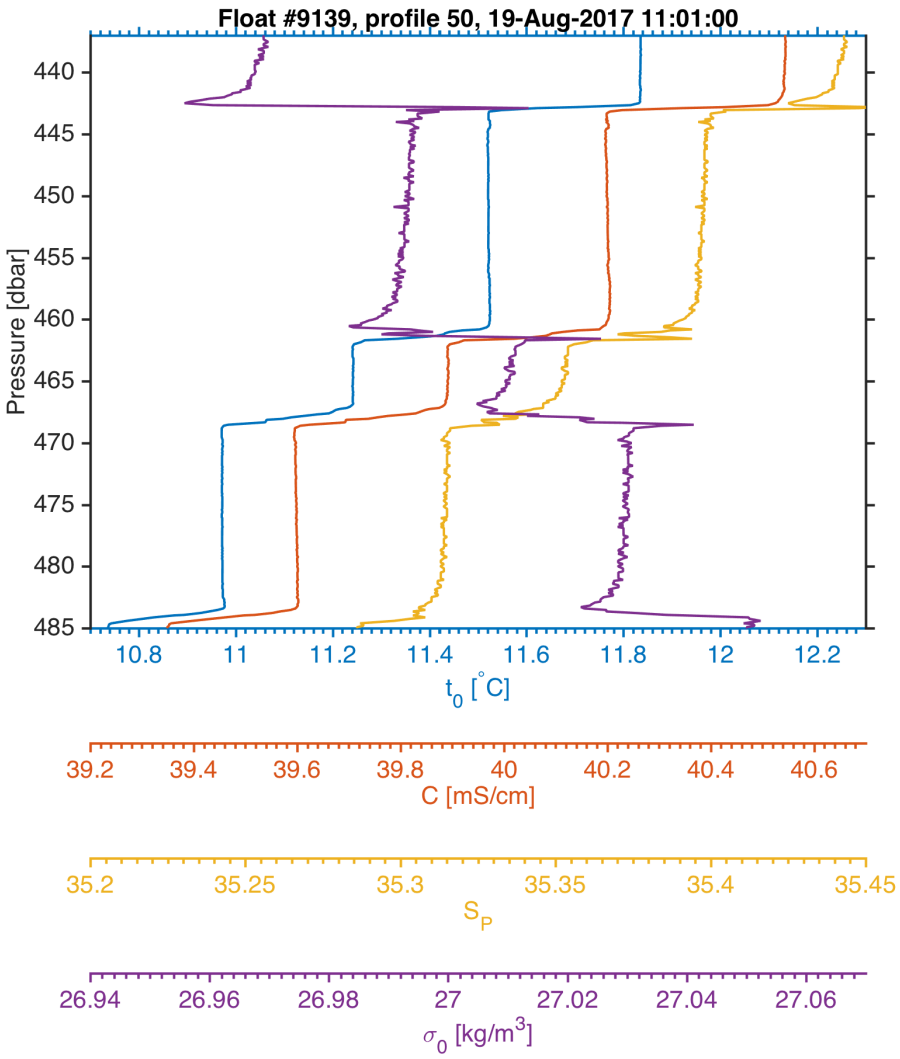

Fig. 2 Measured temperature and conductivity from MRV ALAMO #9139 in the Caribbean Sea. The selection of data shown highlights dynamic errors in temperature and conductivity, and how they propagate into derived values.

This data set illustrates very clearly all three correction time scales important for the RBR*argo* CTD. Plotted are profiles of in situ temperature, conductivity, salinity, and potential density anomaly through three steps from profile 50 (Fig. 2). Signatures of dynamic conductivity errors are most readily found by identifying inversions in potential density anomaly. In this particular example, the density profile is unstable on scales of ~10m (e.g., the complete mixed region between sharp T/S interfaces), ~2m (e.g., at the base of the mixed layers), and ~0.2m (e.g., a sharp spike on top of a mixed layer). At an ascent rate of 10cm/s, the length scale of the instabilities translate into time scales of approximately 100s, 20s, and less than 1s.

As with Lueck and Picklo (1990), we will use data from the T/S staircase to develop and tune algorithms to correct RBR*argo* CTD data for dynamic errors. In this analysis, we utilize profiles 50, 52, and 60 from float 9139, which was specifically reprogrammed by Woods Hole Oceanographic Institution after profile 47 to transmit the raw, full resolution CTD data to better understand the CTD performance.

3 Thermistor thermal inertia

By the reasoning discussed earlier in the introduction, the only factor that causes a short-term error is the finite response time of the thermistor. With that in mind, the solution to correcting the short-term error is to correct temperature.

A number of methods have been developed to reconstruct the true temperature from measured temperature. For example, sharpening the thermistor with discrete filters can advance the temperature and enhance the high frequency signal (e.g., Fozdar et al., 1985; Giles and McDougall, 1986; Lueck and Picklo, 1990). Analogous methods exist in the continuous time domain (Fofonoff et al., 1974). For the specific purpose of matching the response of conductivity and temperature, there exist spectral methods based on transfer functions (Horne and Toole, 1980). Some researchers prefer to "slow down" conductivity instead of "speed up" temperature (e.g., Schmitt et al., 2005)

In terms of solutions, the simplest correction is to shift temperature in time to correct the phase lag. Adjusting the phase will ensure that the conductivity and temperature readings were taken simultaneously. Conductivity is assumed here to be an infinitely fast measurement, and therefore already referenced correctly to time. We can use the ALAMO Caribbean thermohaline staircase data to estimate the optimal time shift. The optimal time shift is expected to be less than one second, therefore it was necessary to resample the data from 1Hz to 10Hz prior to applying a shift. Salinity and potential density anomaly were computed from conductivity and temperature for temperature shifts from ranging from -0.5s to 0.1s (negative values indicate an advancement in time). The resulting salinity and density profiles through a strong density interface are shown below (Fig. 3).

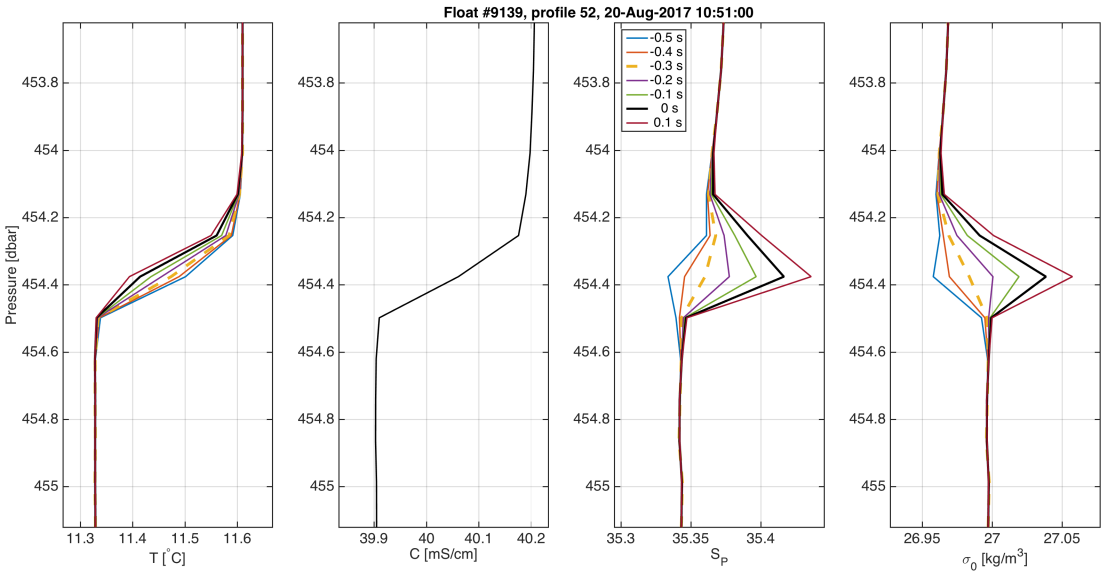

Fig. 3 The impact of shifting temperature in time on salinity spiking. The optimal time lag for temperature minimizes salinity spiking in strong temperature gradients.

As the float ascends through the interface, it encounters increasingly warm and salty water. Without a time shift, salinity and density have positive anomalies at sharp interfaces, indicating that the temperature lags conductivity. A positive time shift, which increases the natural lag, clearly enhances the positive salinity and density spikes. Alternatively, advancing temperature by a relatively large negative value (Δt = -0.5s) causes negative anomalies. The ideal time shift lies between these extremes. To choose the ideal value objectively, the salinity variance of each lag was computed by subtracting a smoothed version of the data from itself, forming a time series of salinity anomaly. The salinity anomaly time series with the lowest variance (i.e., the smallest spikes) was associated a shift of -0.3s. This value is plotted as the dashed line in Fig. 3.

The 0.3s temperature advance was confirmed in two ways. The first method was based on finding the lag at which temperature and conductivity gradients are maximally correlated across a density interface. The second approach was to compute the phase of the transfer function of conductivity relative to temperature (Fig. 4). The slope of the phase curve, dφ/dω, is equal to the time lag between the sensors. The slope of the phase curve was consistent with a 0.3s delay over a range of 0.03Hz to 0.2Hz. This is a relatively low frequency band that is consistent with the approach by which temperature is simply shifted in time (i.e., a "DC" or zero-frequency lag).

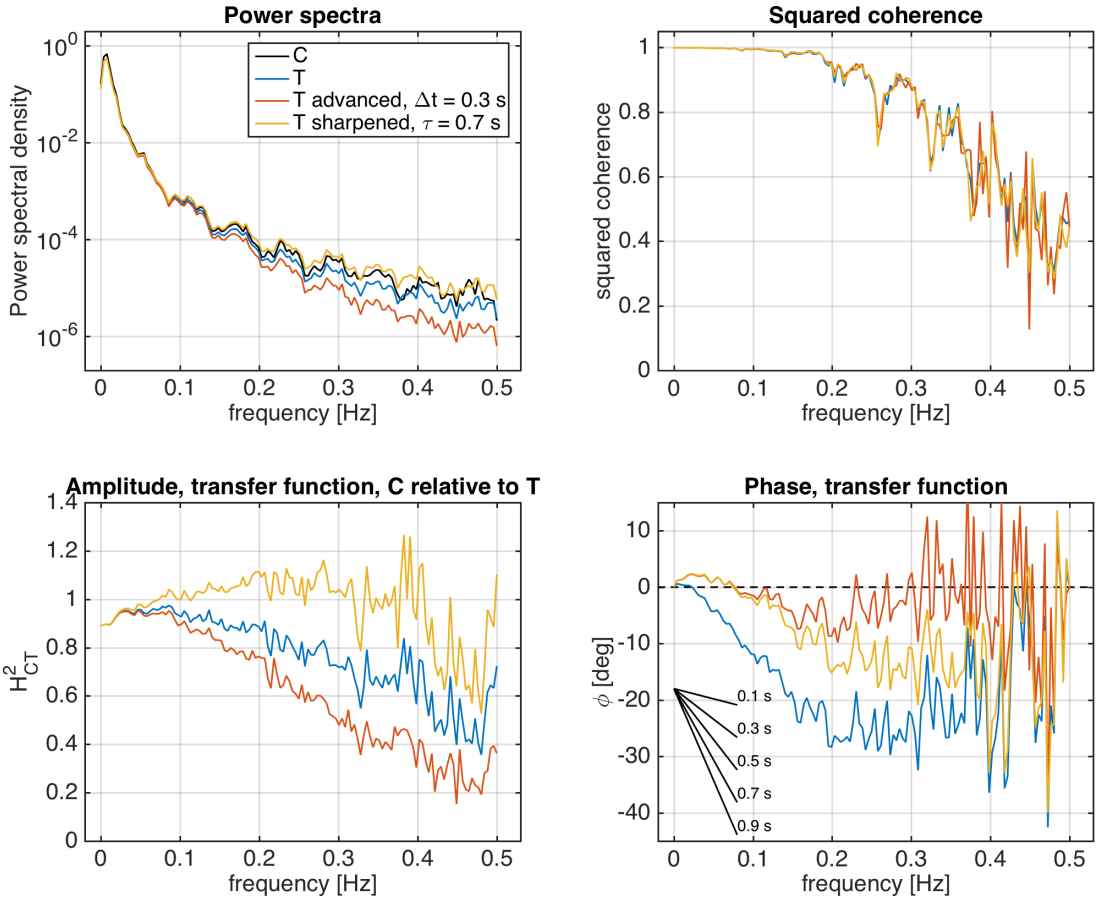

Fig. 4 Cross spectral comparison of conductivity and temperature to assess thermistor correction strategies. Advancing temperature by 0.3s approximates the single-pole sharpening algorithm.

4 Conductivity cell thermal inertia

The density profile from the ALAMO thermohaline staircase data indicated that there were dynamic errors on timescales of 10s and of 60s, which were the results of the medium-term and long-term conductivity thermal adjustments. Here we show that these adjustments originate from the conductivity cell, and present more compelling evidence that there are indeed two time scales. We again rely on the ALAMO thermohaline staircase profiles, but this time present salinity and temperature as functions of time as the float passes through different steps in the staircase (Fig. 5). Temperature and salinity are normalized with their respective values in the previous mixed layer and the current mixed layer. The elapsed time is initialized such that t = 0 coincides to the time when the float exits the first mixed region and enters the base of an interface.

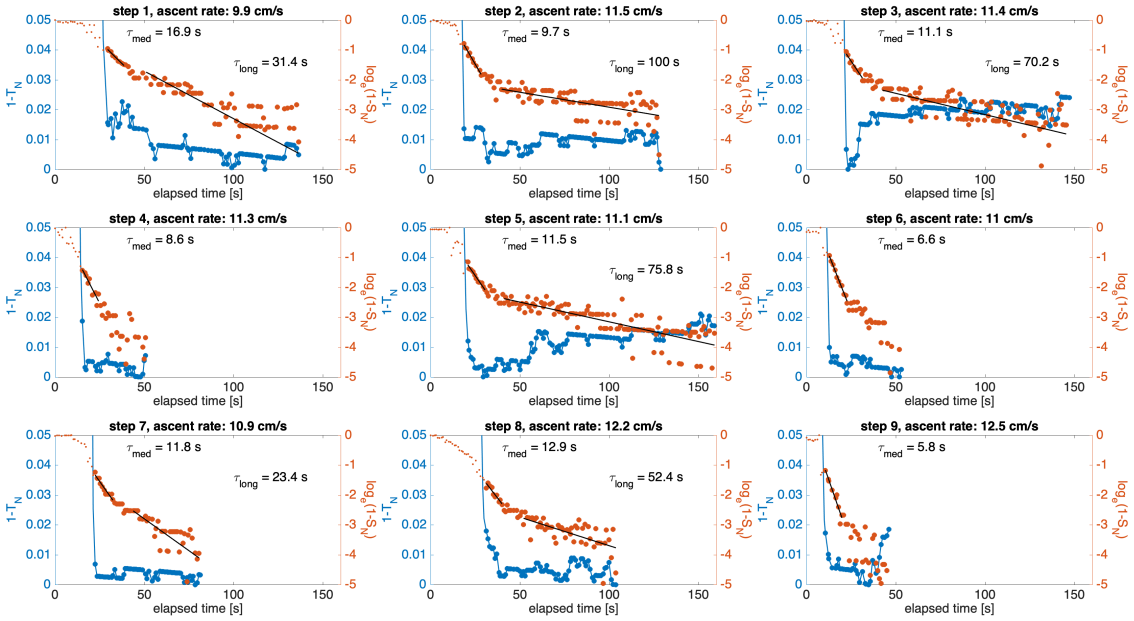

Fig. 5 Time series of normalized temperature and normalized log-salinity through nine thermohaline steps in the same profile. In the thicker steps (1-3, 5, 7, 9), log-salinity is characterized by two decay rates, evident as two distinct linear regions.

Note that steps 4, 6, and 9, were too thin to detect the long-term adjustment. In the remaining steps, the log-transformed salinity could be modelled by two piecewise linear trends. First, normalized salinity decreases steeply in a linear fashion after the CTD enters the mixed layer for about 10s to 20s. After this, salinity decreases at a slower rate until the next time series is truncated at the next interface. The inverse of the slope of each section yields approximate time constants for each adjustment. Fitting a straight line to the period defined by the rapid decrease a time constant of 5.8s to 16.9s, and fitting straight line to the period defined the slower decay yields a time constant of 23s to 100s. Bear in mind that these are rough estimates; a careful measurement of both time constants requires each decay process to be isolated and analyzed independently.

4.1 Long-term thermal adjustment

In order to quantify both thermal time constants, each process must be isolated. This is fairly straightforward because the two adjustment time scales differ by a factor of six. If each process is represented by an exponential decay model, then isolating the long process is a simple matter of considering data after the equivalent of two or more short-term

time constants have passed, or about 20s in this case. After this point, the short-term adjustment error has decayed to 10% its value, and the total transient component of signal is dominated by the longer process.

The existence of the long-term thermal adjustment was known and characterized by RBR before the MRV ALAMO float was launched into the Caribbean. The adjustment was studied in the lab by plunging an RBR CTD into a 1 m deep calibration bath to simulate a step change in temperature. The bath was about 3°C warmer than the ambient air temperature. To ensure the conductivity cell was adequately flushed, the CTD was oscillated vertically in the calibration bath with 40cm vertical amplitude and a peak speed of 10cm/s. Only data with positive speed (descending with flow into the cell at speed 10±1cm/s) was selected for analysis so that the results represent conditions expected for an Argo float.

Immediately after the instrument entered the water, the initial measured conductivity was 53.52mS/cm (Fig. 6). As time progressed, the measured conductivity increased in an exponential fashion, eventually stabilizing at 53.56mS/cm.

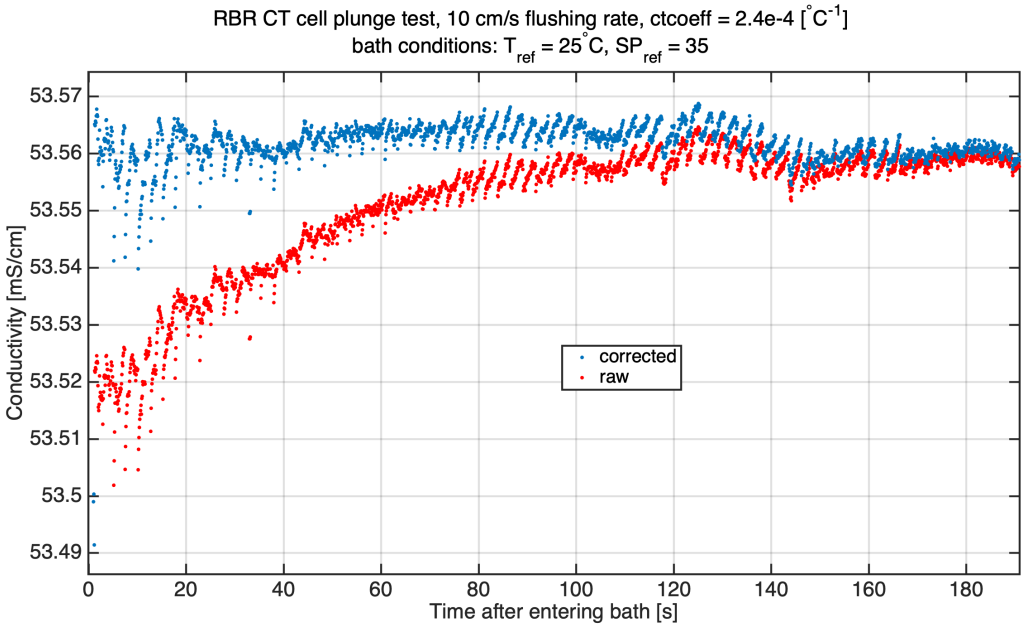

Fig. 6 Calibration lab comparison between uncorrected conductivity and conductivity corrected for long-term thermal adjustment.

At t = 0s, measured conductivity was initially low because the colder CT cell cooled the water it was sensing. Measured conductivity increased as the cell equilibrated thermally with the water.

Instead of modelling the heat exchange process, as was done by Lueck (1990), we can rely on measurements to develop a correction for the conductivity error introduced by the heat exchanged between the conductivity cell and the water. The RBR CT cell contains within it a thermistor. The difference between the internal CT cell temperature and the water temperature is a proxy for the heat flux between the cell and the water. The difference between the internal CT cell temperature and the water temperature is correlated with the conductivity error over the adjustment period, and therefore a correction factor for conductivity that depends on the temperature difference can be devised. The form of the correction factor is

$$C_{cor} = \frac{C_{measured}}{1+ctcoeff*(T_{ctcell}-T_{marine})}$$

where *ctcoeff* is a coefficient with a value determined experimentally.

With the correction model above, the coefficient *ctcoeff* is found by measuring the slope of a line fit to C_{meas}/C_{ref} - 1 against T_{ctcell} - T_{marine} (Fig. 7).

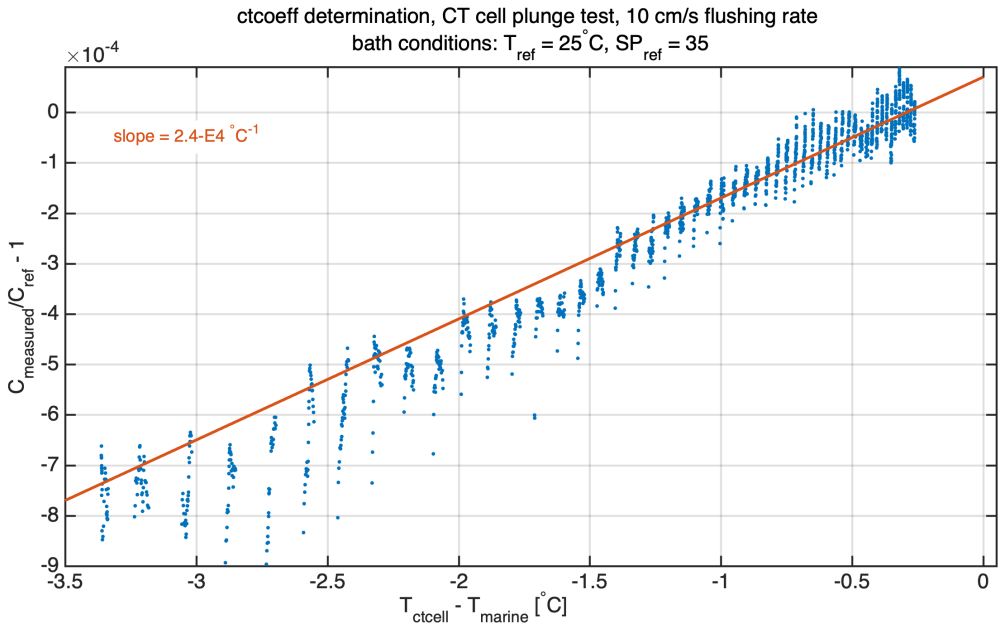

Fig. 7 Parameterization of the long-term thermal adjustment correction factor as a function of the temperature difference between the conductivity cell and the water.

A least squares fit to the regression yields a line with a slope of 2.4e-4°C^{-1}.

The time constant for this adjustment, defined as the time it takes conductivity to reach 63% of the difference between the initial and final values, is 60s. Henceforth, this adjustment is often referred to as the τ_{60} correction.

4.2 Medium-term thermal adjustment

In the Caribbean Sea thermohaline staircase (Fig. 1), the medium-term thermal adjustment was characterized by density inversions with a thickness of 1 or 2m, or 10 to 20s at a rise rate of 10cm/s. In this particular case, the CT cell is ascending from relatively cool water into warmer water. The cell cools the water it is currently measuring, reducing its conductivity. After the float passes through a strong temperature gradient, the medium-term thermal conductivity error translates into a reduction in salinity as high as 0.01. This low salinity artifact causes an apparent density inversion on the same spatial scale with an error of about 0.01kg/m^3 at the base of the steps.

Application of the long-term thermal adjustment correction factor allows us to isolate and characterize in the medium-term adjustment. To correct for the medium-term thermal adjustment, we use the Morison et al. (1994) twist on the Lueck and Picklo (1990) approach. Instead of correcting conductivity for thermal inertia, Morison et al. (1994) compute a correction term that is used to estimate the water temperature in the cell from the measured temperature. The modified temperature is used along with the measured (i.e., *uncorrected*) conductivity to compute salinity. The form of the temperature correction is essentially the same as the Lueck and Picklo (1990) conductivity correction:

$$T_{cor}(n) = -bT_{cor}(n-1) + a[T(n) - T(n-1)]$$

where the *a* and *b* coefficients are the same coefficients used in the conductivity correction, *T* is the water temperature, and T_{cor} is the temperature correction. The temperature correction is then *subtracted* from the water temperature to form an estimate of the temperature in the conductivity cell:

$$T_{cell}(n) = T(n) - T_{cor}(n).$$

The measured conductivity and the estimated temperature in the cell are then used to derive practical salinity.

The advantage of this approach is that it is no longer necessary to calculate γ. Although Lueck and Picklo (1990) assume a constant value for γ, they acknowledge it varies with salinity and temperature. For example, it ranges from 0.91 at T = 5°C S = 35 to 1.04 at T = 25°C S = 35. Thus, for the most accurate correction, γ must be computed for a given temperature and salinity.

The parameters α and β are cell-specific and must be determined for any implementation of the thermal mass correction. These parameters are (mostly unknown) functions of the cell geometry, the heat capacity of the materials in the cell, and the flow speed through the cell. Lueck and Picklo (1990) measure α and β from CTD profiles taken in the Caribbean Sea thermohaline staircase. The ideal values were those that that adjusted the measured profiles to become physically realistic (i.e., free of spikes and density inversions). More recently, other methods have been devised to measure α and β. These approaches typically require either a well-characterized reference profile, an upcast/downcast pair (Morison et al., 1994, Mensah et al., 2008), or simply a careful inspection by eye (Schmitt et al., 2005). The advantage of the Lueck and Picklo (1990) approach is that it does not require reference data or upcast/downcast pairs because the salt-fingering thermohaline staircase has a well-defined structure. Any deviation from the structure is assumed to be attributed to the sensor errors.

We follow the same procedure laid out by Lueck and Picklo (1990) to determine β, which is to measure the decay constant of salinity when the float is in a uniform temperature environment. In the case of a step change in temperature, the simplest model for heat transfer between objects of dissimilar temperature (Newton's Law of Cooling) predicts that the temperature of one object exponentially approaches the other. When conductivity is determined primarily by temperature, and the cell is in constant temperature environment (i.e., after a step change), then it reaches the new conductivity value exponentially in time, i.e., $C = Co(1 - e^{-\beta\tau})$. Thus, the time constant, $\tau = 1/\beta$, can be measured by log transforming the data and measuring the slope of a line fit to the data.

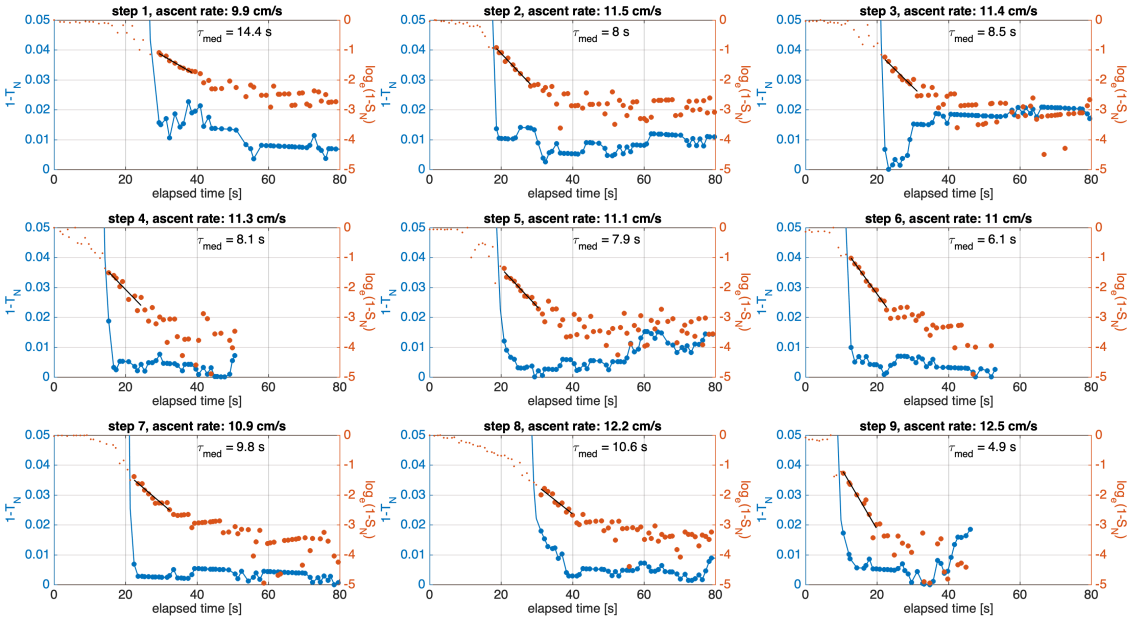

Fig. 8 Time series of normalized temperature and normalized log-salinity in nine thermohaline steps. Salinity was computed after correcting conductivity for the long-term adjustment. The transient salinity response is now governed by the medium-term thermal adjustment.

Following Lueck and Picklo (1990), we fit to log-transformed salinity because in computing salinity the natural pressure dependence of conductivity is removed. Time series of log-scaled normalized salinity, and normalized temperature, from nine steps in the thermohaline staircase, are shown in Fig. 8. The time series starts just as the float enters an interface, and ends before it enters the next interface. The long-term thermal conductivity correction has been applied.

The temperature record reveals that the homogenous layer starts at an elapsed time of about 20s, after which time the log-scaled normalized salinity decreases linearly. At about 35s, the slope flattens, indicating that the cell has adjusted thermally. The normalized temperature provides an indication of the degree to which conductivity is freely decaying, or whether temperature variations are still forcing the signal. In step 8, for example, the temperature decreases slightly immediately after the float passes through the interface, which means that conductivity was forced slightly, and that there is additional uncertainty in the time constant derived from this step. Fitting a line to the data between 20s and 30s yields a measurement of the inverse time constant, β. The median value of the nine time constants measured is 8s, or β = 0.125s-1 (τ = 8s).

The Lueck and Picklo (1990) method to estimate α is somewhat more complex. Here we will simply compute salinity and density for a range of values, and select the one that produces the most physically realistic profiles (i.e., stable staircase structures). This is essentially a qualitative approach to the problem that others have approached statistically by minimizing errors.

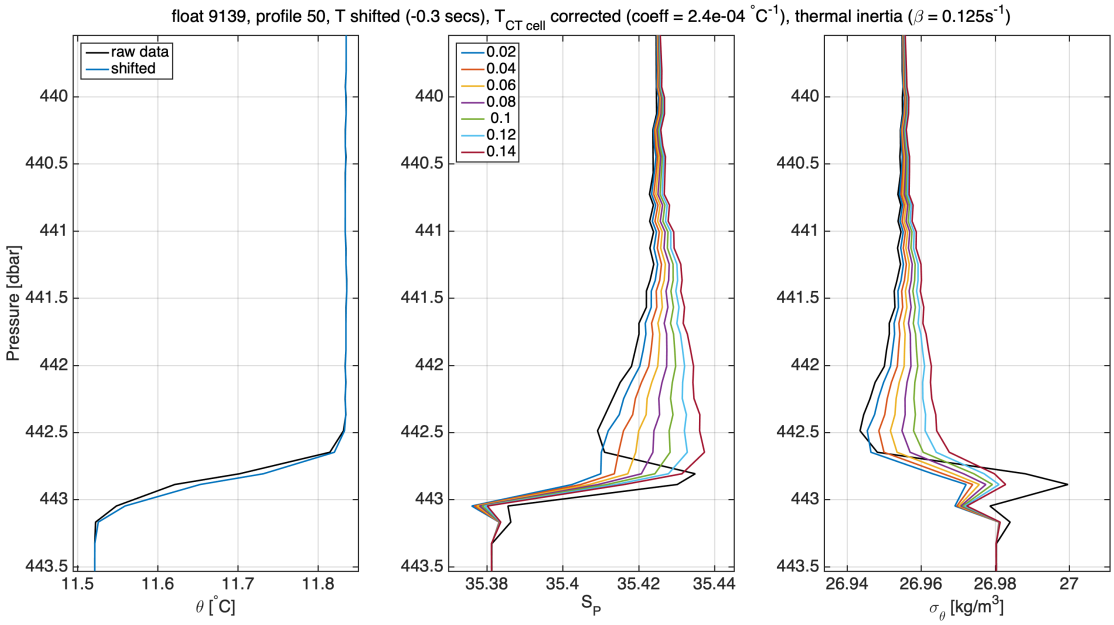

Fig. 9 Effect of the Lueck and Picklo (1990) amplitude parameter (alpha) on salinity and potential density anomaly in one thermohaline step.

Plotted in Fig. 9 are temperature, salinity, and potential density anomaly for 0.02 < α < 0.14. The limits of the parameter space were chosen subjectively. When α is too small, the base of the mixed layer remains unstable. When α is too large, the base of the mixed layer becomes stratified because the correction overcompensates salinity. The ideal value lies in the range of 0.06 to 0.10, and we select the middle of this range, 0.08, as the best estimate because it produces the weakest gradients at the base of the uniform layer.

In summary, the ideal coefficients for the medium-term thermal correction, as determined from the Caribbean thermohaline staircase, are:

α = 0.08

β = 0.125 s^{-1} (τ = 8 s)

5 Validation of the correction algorithms: salinity and density

5.1 Caribbean T/S Staircase

Applying the short-term correction temperature and both thermal conductivity corrections improves the MRV Caribbean profiles by stabilizing the density profiles. A short section of profile 50 containing three T/S steps is shown in Fig. 10. The corrections reduce spiking in salinity and density, and restore stability for much of the density profile shown. For example, the salinity spike at 443dbar, which has a magnitude of roughly 0.01, is eliminated. The density anomaly caused by this salinity spike is nearly 0.02g/kg^3, and it too has nearly vanished. The larger scale inversions, such as that found between 443dbar to 461dbar, are corrected by both thermal conductivity corrections.

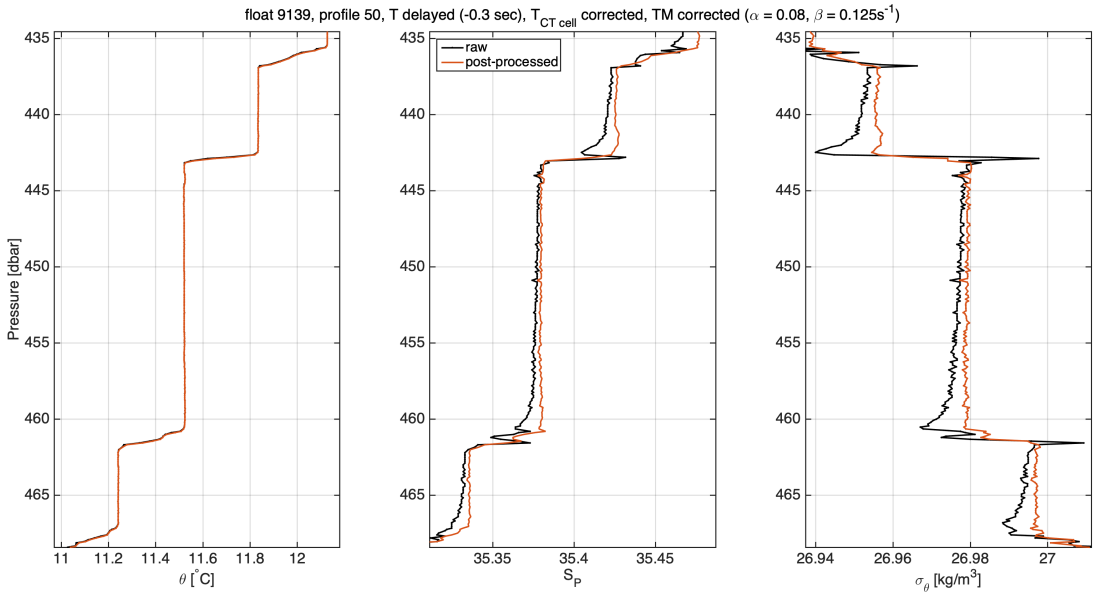

Fig. 10 Comparison of raw and corrected potential temperature, salinity and potential density anomaly. Note how the profiles are stable over a range of spatial scales.

It is evident from Figure 10 that post-correcting temperature and conductivity reduces both the number of inversions and the magnitude of the inversions in one or two T/S steps. However, we wish to quantify the corrections statistically for a full profile to support our choice of correction algorithms and parameters. To do so, we chose another profile from float #9139 that has well defined staircase features. After the corrections were made, the data are averaged into 2dbar intervals to remove noise and therefore the number of spurious inversions. The stratification is continuous and stable above the staircase region, and also already stable without corrections, so we restrict our analysis to the staircase region from 400dbar to 500dbar (Fig. 11).

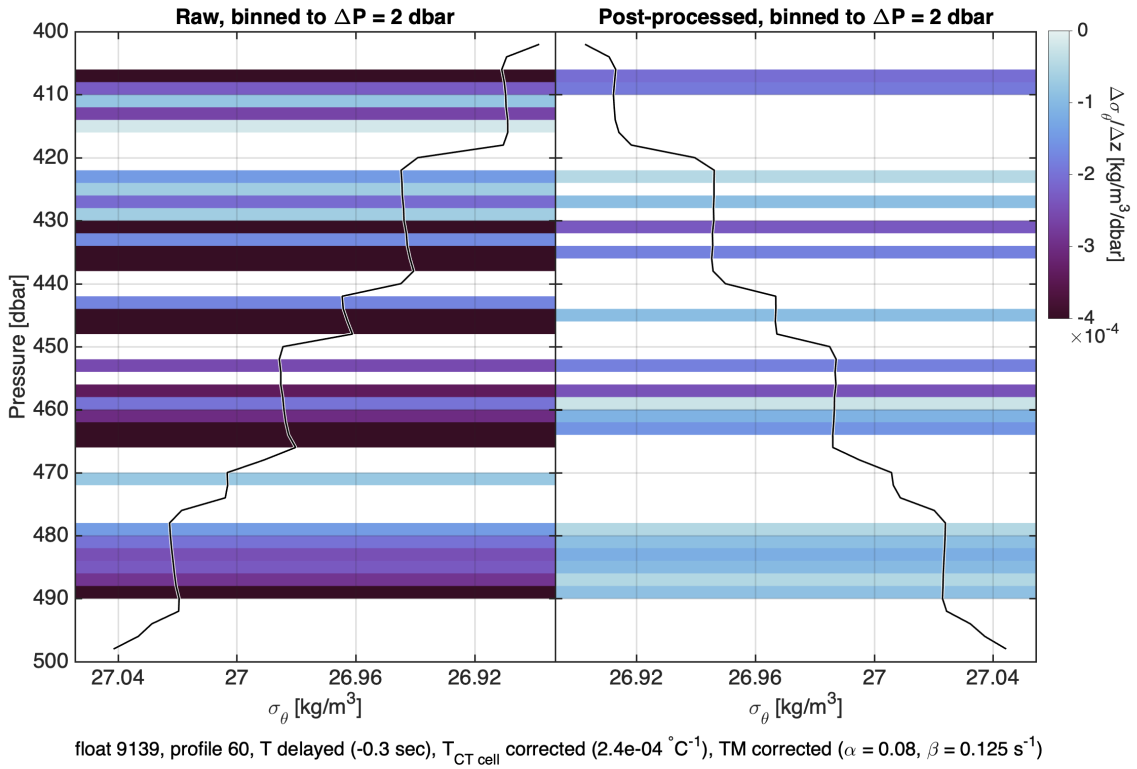

Fig. 11 Assessment of the correction algorithms in terms of the reduction of both the number and magnitude of density instabilities.

Before applying dynamic corrections, 57% of the consecutive points in the thermohaline staircase were unstable, whereas after applying the corrections, only 35% of the consecutive points were unstable. The median value of the instabilities before applying dynamic corrections was 2.44 x 10^{-4} kg/m^3/dbar, whereas the median value of the instabilities after applying dynamic corrections was 1.04 x 10^{-4} kg/m^3/dbar. The median errors in both cases are well below the Argo data quality threshold value allowed for density inversions: 0.03 kg/m^3 (Wong et al., 2015).

Extending this sort of analysis to more profiles from the same float is not particularly insightful. The number and magnitude of the inversions depends to a large degree on the nature of the stratification. Furthermore, all of the factors upon which the dynamic corrections depend, such as conductivity cell geometry, material heat capacity, and ascent rate, are consistent for the all of the profiles collected by float #9139.

5.2 Validation on independent datasets

5.2.1 North Atlantic Ocean MRV/RBR ALAMO floats

The correction algorithm parameters were determined from a small segment of a profile through the Caribbean Sea thermohaline staircase made by an RBR*argo* MRV ALAMO float. Perhaps unsurprisingly, applying the correction algorithms to a different profile from the same float improved that profile by reducing the number and magnitude of the density inversions. As argued above, extending that type of analysis is not helpful because the results depend on

the stratification. We can, however, at least verify that the corrections are reasonable by applying them to other float data collected with the RBR*argo* CTD.

In September 2018, ten MRV ALAMO floats with RBR*argo* CTDs were air-deployed by the US Naval Academy and the Woods Hole Oceanographic Institution from a US Air Force Hurricane Hunter aircraft into the North Atlantic Ocean approximately 1200km east of Florida. The floats profiled on ascent from 300dbar to the surface up to 15 times per day. The average ascent rate was 0.11m/s, although instantaneous rates ranged from 0.09 to 0.13m/s. The CTD sampled at 1 Hz, but the data were averaged into pressure bins of width 1dbar prior to telemetry. These floats were equipped with the same model of CT cell that was installed on float #9139 which profiled through the T/S staircase.

Conductivity and temperature were corrected for the medium and long-term thermal errors. Bin averaging effectively lowered the sampling interval to 10s ($\Delta t = p \div dp/dt = 1dbar \div 0.1dbar/s = 10$ s), and therefore the data were upsampled to 1Hz so that the medium term thermal correction (τ_8) could be meaningfully computed. The short-term temperature lag correction was not applied given the relatively low effective sampling rate.

A single profile from each float was selected visually to demonstrate the impact made by the corrections. In particular, profiles with surface mixed layers lying above strong temperature gradients were chosen (Fig. 12). As with the staircase profiles, is relatively easy to demonstrate the efficacy of the corrections because, in homogenous water, it is assumed any deviation from uniformity is caused by dynamic adjustments.

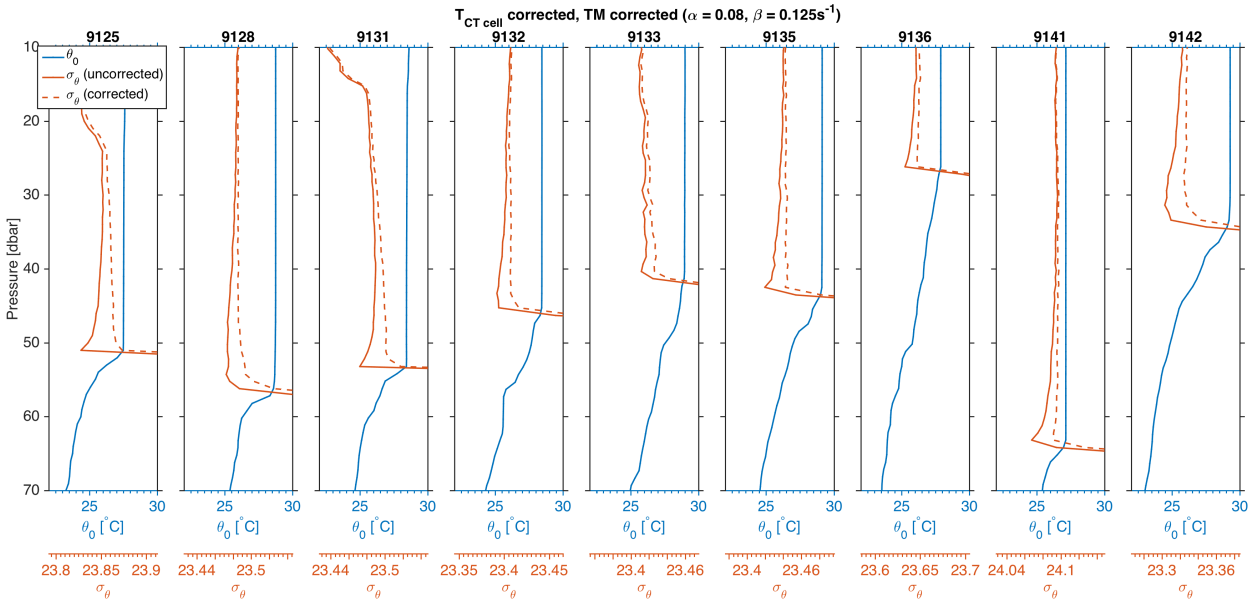

Fig. 12 Density profiles in the surface mixed layer before and after applying dynamic corrections. These RBRargo MRV ALAMO floats were deployed simultaneously in the North Atlantic Ocean, 1200 km east of Florida.

Density is analyzed here because it provides a physical constraint on the corrections. When uncorrected, the mixed layers in these profiles are dynamically unstable with the largest inversions occurring at the base. In all nine profiles shown, the dynamic corrections bring the density profile closer to neutral stability. The magnitude of the correction depends on the strength of the temperature gradient. For example, in the case of the profile plotted from float #9125 (Fig. 12), the density correction reaches 0.04kg/m^3 after passing through 3m of a 1°C/m gradient. The dynamic density error decreases with time after the float enters the mixed layer because the conductivity error is no longer being forced by a temperature gradient.

Quantitatively evaluating how well a single set of coefficients (derived from a single float) applies to other RBR*argo* CT cells is not straightforward, particularly when the validation data set originates from in situ profiles. The reason is that the nature of the stratification critically impacts the existence and magnitude of inversions. Some uncorrected profiles are stably stratified, while others are not. As an illustration, consider two identically-equipped floats, each sampling a

different region. One float repeatedly samples the surface mixed layer in a thermally stratified region (e.g., the subtropics), and the uncorrected data produces an unstable water column. The second float repeatedly samples samples a salt-stratified region with weak temperature gradients (e.g., high latitude fjords), and the uncorrected data produce a stable water column. The two floats will give two very different results if the efficacy of the corrections is evaluated by the number and magnitude of density inversions in the profiles. A comparison made with these metrics is essentially meaningless.

5.2.2 Japan Argo #2903005

A pair of TWR Apex floats with RBR*argo* CTDs were deployed from the R/V Keifu Maru on February 3, 2018 at 28°N 165°E in the North Pacific. The platform numbers of these floats are #2903005 and #2903327, and the data are made available on the GDACs under the Argo RBR Global Pilot Program. These floats provide another opportunity to validate the dynamic correction algorithms and parameters, but this time at 2dbar resolution. To implement the corrections, it was necessary to go back to the binary science log files transmitted by the float because the GDAC NetCDF files do not contain the CT cell internal temperature.

For this particular example, we chose cycle 90 from float #2903005 because the profile measured during this cycle is characterized by a uniform mixed layer underlain by a strong temperature gradient (Fig. 13). All measured and derived fields indicate that the mixed layer reaches down to a pressure of 80dbar. The CT cell internal temperature, which is the basis for the τ_{60} thermal conductivity correction, is also included to illustrate how it lags water temperature. The impact of the dynamic errors is evident at the base of the mixed layer, where there is a negative anomaly in salinity of about 0.015.

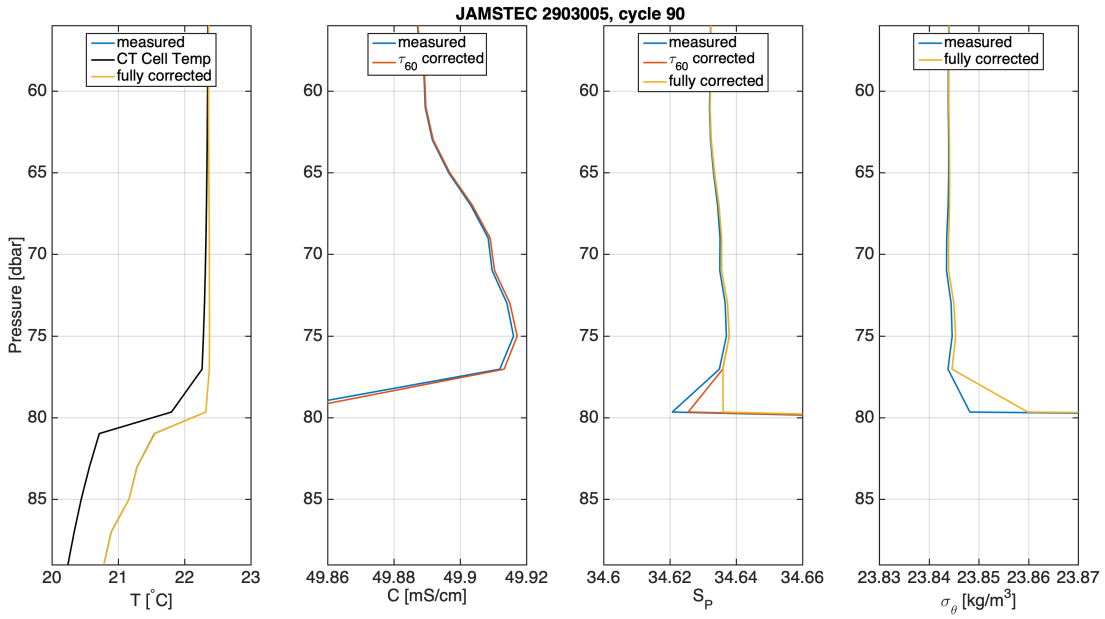

Fig. 13 Illustration of how the dynamic corrections impact temperature, conductivity, salinity, and potential density from Japan Argo float 2903005, profile 90.

Measured temperature was advanced to account for the thermistor lag, however, the impact of the shift is not easily visible on the scale shown on Fig. 13. The temperature lag from the thermistor is large enough to cause a temperature difference of 0.006°C at the based of the mixed layer (not shown), but less than 0.002°C elsewhere. The temperature advance and long-term thermal conductivity correction decrease the salinity error by about 0.005, and then the τ_8 correction further decreases the maximum error at the spike by 0.010. The net result of all three corrections is that salinity is now uniform at the base of the mixed layer, and density is more stably stratified.

One important point to note here is that it was necessary to upsample the data with interpolation to implement the thermistor lag correction and the Lueck and Picklo τ_8 correction. In the case of the thermistor inertia correction, the interpolation *method* (e.g., linear or spline) has a small effect on the corrections. In Fig. 13, linear interpolation was used. However, if splines are used, the salinity spike is not reduced to the same extent. With that in mind, we conclude that this dataset supports the dynamic corrections and parameters we developed, however data bin averaged to 2dbar are not of sufficient resolution to scrutinize the value of the coefficients.

6 Discussion

6.1 Magnitude of the corrections

The size of the corrections depends on the strength of the temperature gradient and the temperature history experienced by the float. To provide a bulk summary of how large the corrections are as a function of temperature gradient, both thermal conductivity corrections were applied to MRV/RBR*argo* float #9142 from the North Atlantic Ocean deployment. The instantaneous difference between the corrected and uncorrected density, plotted as a function of the temperature gradient in °C per 2dbar is shown in Fig. 14.

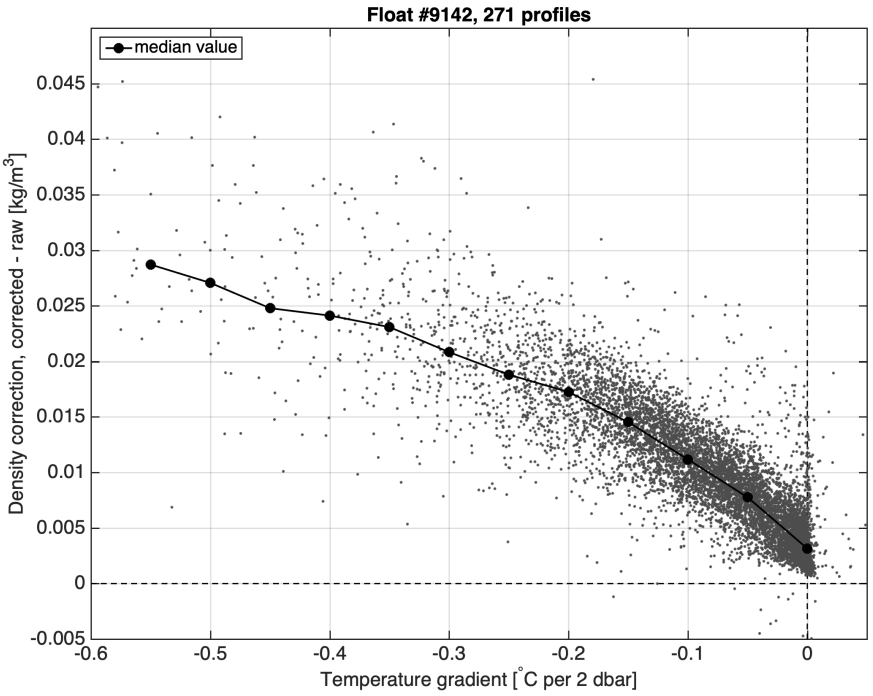

Fig. 14 Density correction as a function of vertical temperature gradient for MRV/RBRargo float #9142 in the North Atlantic. On ascent the floats encounter increasingly warm water, and dynamic errors in conductivity cause density to be underestimated.

It is important to note that the finite time required for a the conductivity cell to equilibrate thermally means that it is possible for the density correction to be finite when there is no temperature gradient. This "memory" in the correction is responsible for some of the scatter in Fig. 14, as well as the non-zero correction when dT/dP = 0.

As expected, the size of the density correction increases with the strength of the temperature gradient. A temperature gradient of -0.1°C/2dbar will create an error of 0.01kg/m^3, while a much stronger gradient of -0.5°C/2dbar will create an error of about 0.027kg/m^3. It is clear from Fig. 14 that these numbers are uncertain at the level of about 50%; but this uncertainty is dominated not by the degree to which the corrections are appropriate for this float, but rather by the auto correlation caused by the time history of the corrections.

6.2 Thermistor response correction

In this study, we chose to simply advance temperature in time by 0.3s to account for the phase lag of the thermistor. While quite effective, simply lagging temperature overlooks the fact that the thermistor inertia not only delays the measurement, but also reduces natural high-frequency temperature variability. Strictly speaking, both the phase and amplitude response of the thermistor depend on frequency.

Numerous algorithms have been developed to apply a frequency-dependent correction for both amplitude and phase. One such algorithm is based on a model of the heat exchange between the thermistor and the water, which is approximated by Newton's Law of Cooling. The mathematics required to transform the law of cooling in to a digital corrective algorithm can be found in Fozdar et al. (1985). The effect of the Fozdar et al. (1985) correction algorithm is to enhance the signal amplitude at high frequencies, and to modify the phase in order to reconstruct the true temperature. The correction algorithm is a type of single-pole high-pass filter in the parlance of signal processing. The correction algorithm depends on sampling rate, and has one free parameter: the thermistor time constant.

$$R_k = \frac{1}{1-a}(S_k - aS_{k-1})$$
$$a = e^{-\Delta/\tau}$$

where Δ is the sample interval and τ is the thermistor time constant. The downside of this algorithm, which is common to other "sharpening" algorithms, is that the derivative term amplifies noise from the input signal, and so quite often the reconstructed signal is subsequently smoothed. In fact, the Fozdar et al. (1985) algorithm includes a smoothing term for this purpose. The smoothing term is precisely the inverse operation of sharpening, and it is only useful if the sampling rate is much higher than the desired smoothing time constant. This is not the case for an RBR*argo* CTD sampling at 1Hz, and we therefore neglect the term.

Some researchers (e.g., Johnson et al. 2007; Martini et al., 2019) prefer to use the continuous form of the correction algorithm:

$$T = T_m + \tau \frac{dT_m}{dt}$$

where T_m is the measured temperature, T is the true temperature, and τ is the thermistor time constant (Fofonoff et al., 1974). Unfortunately, while conceptually simple, this algorithm does not allow one to control the filter cutoff frequency, and it may be computationally inefficient because one must fit *N* previous points to estimate the temperature gradient.

The Fozdar et al. (1985) algorithm was tested on the RBR*argo* MRV Alamo Caribbean data set, and the reduction in salinity spiking was clear. However, with one free parameter (the filter time constant), it was not possible to adequately recover both the phase and the amplitude. Phase is the most important factor for reducing salinity spikes, and when the filter time constant was optimized for phase, the amplitude response became unrealistic. In comparison, simply advancing the temperature by 0.3s recovered the phase but without overcorrecting the amplitude.

There are other downsides to the Fozdar et al. (1985) algorithm. The filter becomes increasingly sensitive to sample rate when sampling rate is about the same as the thermistor time constant. In the case of the RBR*argo* CTD in the Caribbean, the sampling rate was 1Hz, and the thermistor time constant was measured by plunge tests to be about 700ms. Schmitt et al. (2005) find that the algorithm does not provide an adequate phase shift in this case. Instead, they recommend a different expression for the filter coefficient, *a*, or using a different transfer function discretization scheme based on the bilinear transform (e.g., Bittig et al., 2017).

Evaluation of different algorithms to reconstruct the true temperature requires additional research, and until all of the correction algorithms are evaluated, we simply recommend advancing temperature by 0.3s.

6.3 Flow speed dependence

The RBR inductive CTD operates without pumps; instead the flow generated by the motion of the float flushes the conductivity cell. The parameters α and β in the Lueck and Picklo thermal inertia correction term are known to depend on inversely on flow speed, as is the coefficient *CTcoeff* in the τ_{60} correction. Thermistor time constants are also known to depend on flow rate past the sting. The value of α, β, and Δt for the RBR*argo* CTD was calculated from the Caribbean MRV ALAMO float ascending at a measured rate of 11cm/s, while *CTcoeff* was computed from a CTD moving at 10cm/s. These rates match closely with the nominal Argo float ascent rate of 9cm/s. However, the actual float ascent rate can vary from 6 to 12 cm/s (see ref. in Johnson et al., 2005), and this may have a measurable impact on the coefficient values. We are currently analyzing a number of different datasets to understand the sensitivity of the correction coefficients to float ascent rate. For example, a series of profiles were taken recently in the double diffusion tank at WHOI, which has been used by various researchers to quantify the flow rate dependence of dynamic correction parameters (Schmitt et al., 2005; Martini et al., 2019). Data were collected over a range of profiling rates near the nominal Argo float ascent rate: 5, 10, and 15 cm/s.

6.4 Does the Lueck and Picklo algorithm work for the long-term adjustment?

Some testing (not detailed in this report) showed that applying the Lueck and Picklo (1990) algorithm to conductivity with the parameters α = 0.015, $\beta = 0.0167 s^{-1}$ (τ = 60s) resulted in a corrected measurement nearly identical to when conductivity was corrected with the τ_{60} long-term CT cell correction. This raises the obvious question: If the long-term dynamic conductivity error is the result of heat exchange between the cell and the ambient water, then why not correct for it using the Lueck and Picklo (1990) algorithm?

The decision to use the CT cell temperature correction was the result of practical considerations. The first is that the CT cell correction algorithm does not require the marine thermistor temperature history to initialize. The Lueck and Picklo approach requires the CT cell to be equilibrated to the water temperature in order to make the initial condition, which is typically that $T_{cor}(1) = 0$, an accurate representation of the correction. If not, then the algorithm will require a few time constants (i.e., minutes) to produce a realistic correction. On the other hand, the CT correction uses instantaneous measurements. The temperature "history" of the cell is contained within the internal CT cell temperature record.

There is an important consequence to the fact that the Lueck and Picklo (1990) model is appropriate for the long-term adjustment, which is that conductivity can be post-corrected *without* a record of the internal CT cell temperature. This means that data from floats deployed before the long-term thermal adjustment correction was implemented in firmware can be corrected by DACs using the marine temperature and salinity.

6.5 Application of the dynamic corrections in post-processing

6.5.1 Post-processing at Δp = 2dbar resolution

Ideally, the dynamic corrections should be applied to the data at native resolution (usually 1Hz). At this resolution, the correction for the thermistor time lag and the corrections for the conductivity cell thermal mass can all be applied meaningfully. RBR is working to implement these corrections into the CTD firmware.

However, if the data were not corrected on-board the float, it is still possible to apply some of them in post-processing. A rgo float data is often averaged from a native resolution of 0.1dbar (1Hz at 10cm/s) into 2dbar pressure bins onboard the float for the purpose of reducing telemetry costs. When float data is binned to 2dbar pressure intervals, the effective sampling period becomes about 20s for a 10cm/s ascent rate. Such a coarse resolution has implications for the efficacy of the dynamic error corrections described here. While 20s intervals may be sufficient to meaningfully apply

the τ_{60} long-term thermal conductivity correction, it is too coarse to apply the τ_8 medium-term thermal conductivity correction and the thermistor thermal lag correction, at least in a straightforward manner.

Although the effective sampling interval after binning to 2dbar is more than twice the medium-thermal adjustment time constant (8s), upsampling the data in post-processing prior to applying the correction algorithm is still effective. For example, the thermal inertia script written by G. Johnson (PMEL), which applies the Morison et al. (1994) version of the Lueck and Picklo (1990) correction, upsamples the data to 1Hz. The high-resolution MRV/RBR*argo* Caribbean data allows us to test how well the τ_8 correction works at 1Hz and at 2dbar. A comparison of salinity calculated from raw 1 Hz corrected data (i.e., simulating on-board corrections) to salinity calculated from post-corrected 2dbar data (i.e., post hoc correction) shows that there are only minor salinity differences (~0.002) between the two methods in the thermohaline staircase region of the MRV/RBR*argo* Alamo profiles. Although the difference in salinity between correcting on-board in firmware and correcting on-shore in post-processing is relatively small, the recommendation is still to apply the corrections on-board at the native resolution.

Finally, if the CT cell internal temperature is not available in post-processing because it was not telemetered by the float, then the τ_{60} error can be corrected with the Lueck and Picklo (1990) model as discussed in Section 6.4.

6.5.2 Post-processing at 1 Hz or higher

High frequency data is preferred because the thermistor inertia lag can be meaningfully corrected. The thermistor time advance is 0.3s, and so data acquired at longer intervals will need to be interpolated onto shifted timestamps, or upsampled onto evenly-spaced timestamps with a sample spacing sufficient to shift temperature by an integer number of samples. Either way interpolation is required.

7 Example Matlab scripts to post-correct dynamic thermal errors

7.1 Argo float data bin averaged to 2dbar

In the Matlab code block below, it is assumed that one has access to T_{ctcell}. This data is not available in the GDAC netcdf files, however DACs will be able to find it in the files transmitted by the float providing it was configured thusly.

```
%% variable definitions

%% measured variables
% tmeas  :  measured temperature
% tctmeas:  measured internal temperature inside CT cell
% pmeas  :  measured sea pressure
% smeas  :  measured salinity
% time   :  elapsed time in seconds

%% corrected variables
% tcor  : temperature corrected for thermistor inertial mass
% ctau60: conductivity adjusted for tau60 thermal error
% stau60: salinity adjusted for tau60 thermal error
% scor  : salinity corrected for conductivity cell dynamic errors

%% Coefficients
deltat = 0.3;       % temperature time shift in seconds for thermistor inertial mass
ctcoeff = 2.4e-4;   % long-term thermal coefficient ("tau_60")
alpha = 0.08;       % medium-term thermal magnitude (Lueck and Picklo, 1990)
tau = 8;            % medium-term thermal timescale, 1/beta (Lueck and Picklo, 1990)

%% advance temperature by 0.3 sec to account for thermistor inertial mass
deltat = 0.3;
tcor = interp1(time,tmeas,time + deltat);

%% Calculate conductivity from salinity, temperature, and sea pressure
cmeas = gsw_C_from_SP(smeas,tmeas,pmeas);

%% Apply CT cell internal temperature dynamic correction
ctau60 = cmeas ./ ( 1 + ctcoeff*(tctmeas - tcor) );

%% Derive salinity because it is required by cell thermal mass code
stau60 = gsw_SP_from_C(ctau60,tcor,pmeas);

%% Apply the Morison et al. (1994) version of the Lueck and Picklo (1990)
% thermal inertia correction.  The Matlab function to apply the TM
% correction was written by Greg Johnson (NOAA/PMEL), originally called
% "celltm_sbe41.m". Note: requires elapsed time in seconds ("time") since
% ascent began. celltm resamples to 1 Hz before computing the thermal
% inertia correction.
scor = celltm(stau60,tcor,pmeas,time,alpha,tau);
```

7.2 High-resolution data (~ 1 Hz)

As with the Argo code above, it is assumed that T_{ctcell} was recorded.

```
%% variable definitions
%% measured variables
% tmeas  :  measured temperature
% tctmeas:  measured internal temperature inside CT cell
% cmeas  :  measured conductivity
% pmeas  :  measured sea pressure
% smeas  :  measured salinity
% time   :  timestamp in seconds
% fs     :  sampling rate

%% corrected variables
% tcor  : temperature corrected for thermistor inertia
% ctau60: conductivity adjusted for tau60 thermal error
% scor  : salinity corrected for thermistor and conductivity cell dynamic errors

%% Coefficients
deltat = 0.3;      % short-term temperature advance time in seconds
ctcoeff = 2.4e-4;  % long-term thermal ("tau_60")
alpha = 0.08;      % medium-term thermal magnitude (Lueck and Picklo, 1990)
beta = 0.125;      % medium-term thermal inverse time constant, 1/tau_8 (Lueck and
Picklo, 1990)
fn = fs/2;         % Nyquist frequency (half of logger sampling rate, fs)

%% Calculate conductivity from salinity, temperature, and sea pressure
cmeas = gsw_C_from_SP(smeas,tmeas,pmeas);

%% advance temperature by delta_t = 0.3s to get tcor
tcor = interp1(time,tmeas,time + deltat);

%% Apply CT cell internal temperature dynamic correction
ctau60 = cmeas ./ ( 1 + ctcoeff*(tctmeas - tcor) );

%% Apply the Morison et al. (1994) version of the Lueck and Picklo (1990) correction
a = 4 * fn * alpha * (beta^-1) * (1 + 4 * fn * beta^-1)^-1;
b = 1 -  2 * a * alpha^-1;

% tadj: temperature anomaly needed to estimate water temperature inside CT cell hole
tadj = zeros(size(tcor));
for n=2:length(tcor),
  tadj(n) = -b * tadj(n-1) + a * ( tcor(n) - tcor(n-1) );
end
tcell = tcor - tadj;

%% compute Practical Salinity from tau60 corrected conductivity,
% estimated water temperature in CT cell, and measured pressure
scor = gsw_SP_from_C(ctau60,tcell,pmeas);
```

8 Acknowledgements

RBR would like to thank Drs. Elizabeth Sanabia (US Naval Academy) and Steven Jayne (Woods Hole Oceanographic Institution) for providing the MRV/RBR*argo* ALAMO float data used in this report. Alex Ekholm (WHOI) supported the float deployments, data decoding and processing. Breck Owens (WHOI) initially notified us that there was an MRV/RBR*argo* ALAMO float in the staircase region, and Pelle Robbins (WHOI) shared a Matlab script to read the float list files. Finally, RBR would like to thank Shigeki Hosoda (JAMSTEC) for providing the science binary logs from Japan Argo float #2903005.

9 References

Bittig, H. C. and Kortzinger, A. (2017). Technical note: Update on response times, in-air measurements, and in situ drift for oxygen optodes on profiling platforms. Ocean Science, 13(1):1–11.

Fofonoff, N. P., Hayes, S., and Millard, R. C. (1974). W.H.O.I./Brown CTD microprofiler: methods of calibration and data handling. Technical report, Woods Hole Oceanographic Institution.

Fozdar, F. M., Parkar, G. J., and Imberger, J. (1985). Matching temperature and conductivity sensor response characteristics. *Journal of Physical Oceanography*, 15(11):1557–1569.

Giles, A. B. and McDougall, T. J. (1986). Two methods for the reduction of salinity spiking of CTDs. *Deep Sea Research Part A. Oceanographic Research Papers*, 33(9):1253 – 1274.

Horne, E. P. W. and Toole, J. M. (1980). Sensor response mismatches and lag correction techniques for temperature-salinity profilers. *Journal of Physical Oceanography*, 10(7):1122–1130.

Johnson, G. C., Toole, J. M., and Larson, N. G. (2007). Sensor corrections for Sea-Bird SBE-41CP and SBE-41 CTDs. *Journal of Atmospheric and Oceanic Technology*, 24(6):1117–1130.

Lueck, R. G. (1990). Thermal inertia of conductivity cells: Theory. *Journal of Atmospheric and Oceanic Technology*, 7(5): 741–755.

Lueck, R. G. and Picklo, J. J. (1990). Thermal inertia of conductivity cells: Observations with a Sea-Bird cell. *Journal of Atmospheric and Oceanic Technology*, 7(5):756–768.

Martini, K. I., Murphy, D. J., Schmitt, R. W., and Larson, N. G. (2019). Cor- rections for pumped SBE 41CP CTDs determined from stratified tank experiments. *Journal of Atmospheric and Oceanic Technology*, 36(4):733–744.

Mensah, V., Le Menn, M., and Morel, Y. (2009). Thermal mass correction for the evaluation of salinity. *Journal of Atmospheric and Oceanic Technology*, 26(3):665–672.

Morison, J., Andersen, R., Larson, N., D'Asaro, E., and Boyd, T. (1994). The correction for thermal-lag effects in Sea-Bird CTD data. *Journal of Atmospheric and Oceanic Technology*, 11(4):1151–1164.

Schmitt, R. W., Millar, R. C., Toole, J. M., and Wellwood, W. D. (2005). A double-diffusive interface tank for dynamic-response studies. *Journal of Marine Research*, 63:263–289.

Wong, A., Keeley, R., and Carval, T. (2020). Argo quality control manual for CTD and trajectory data. Report, USA, FRANCE.

10 Revision History

Date	Revision	Description
2020/04/09	A	Revision based on comments from Steve Jayne (WHOI) and Beth Sanabia (US Naval Academy).